

An investigation on the preparation of nanocrystalline hydrous zirconia from zirconium tungstate

M. Antunes · C. A. Perottoni · D. Gouvêa · G. Machado · J. E. Zorzi

Received: 15 June 2017 / Accepted: 29 December 2017 / Published online: 31 January 2018
© Springer Science+Business Media B.V., part of Springer Nature 2018

Abstract Hydrous nanocrystalline zirconia was prepared from an unusual precursor—the bimetallic oxide zirconium tungstate (ZrW_2O_8)—in alkaline medium. Different experimental conditions (NaOH concentration, time and temperature) were used to investigate the effects on crystallographic, morphological, chemical and thermal characteristics of the products. The resulting materials are composed of particles with a crystal structure similar to that of cubic ZrO_2 (or a mixture of tetragonal and cubic phases, depending on the synthesis conditions), with particle size around 5 nm and crystallites around 3 nm in diameter. These particles form high surface area agglomerates, exhibiting mesoporosity and capacity for adsorption of water and carbon dioxide. The synthesis mechanism appears to be constituted, first, by a

chemical substitution reaction between the WO_4 tetrahedra and hydroxyl ions, with subsequent solubilization of the structure. Indeed, excess hydroxyls in the medium form colloidal zirconium ions which polymerize/condense, generating crystalline nuclei in a process facilitated by heterogeneous nucleation and supersaturation. The presence of residual tungsten in all samples appears to be a key element for stabilizing the size and crystalline structure of the materials produced.

Keywords Nanocrystalline hydrous $ZrO_2 \cdot ZrW_2O_8$ · Synthesis mechanism · Alkaline medium · Mesoporosity · Adsorption

Electronic supplementary material The online version of this article (<https://doi.org/10.1007/s11051-017-4119-9>) contains supplementary material, which is available to authorized users.

M. Antunes
Instituto Federal de Educação, Ciência e Tecnologia do Rio Grande do Sul, Vacaria, RS 95200-000, Brazil

C. A. Perottoni · J. E. Zorzi (✉)
Universidade de Caxias do Sul, Caxias do Sul, RS 95070-560, Brazil
e-mail: jezorzi@ucs.br

D. Gouvêa
Universidade de São Paulo, São Paulo, SP 05508-030, Brazil

G. Machado
Centro de Tecnologias Estratégicas do Nordeste, Recife, PE 50740-540, Brazil

Introduction

Zirconium oxide, or zirconia (ZrO_2), is a ceramic material with a broad range of technological applications. At room pressure, ZrO_2 has three polymorphs: monoclinic (m - ZrO_2) (from room temperature to 1170 °C), tetragonal (t - ZrO_2) (from 1170 to 2270 °C) or cubic (c - ZrO_2) (from 2270 °C to its melting temperature) (Patil et al. 2008). The tetragonal and cubic polymorphs are only stable at high-temperature but can be stabilized at room temperature by forming solid solutions with some oxides (Stevens 1986; Hammink et al. 2000).

Metastable tetragonal zirconia has excellent mechanical properties with applications ranging from extrusion dies, cutting tools to bio-implants (Shukla and Seal 2005; Manicone et al. 2007). Cubic zirconia has a high oxygen mobility and found applications as electrolyte in

oxygen sensors and solid oxide fuel cells (Shukla and Seal 2005). Nanocrystalline zirconia exhibits different phase stability allowing the tetragonal and cubic phases be retained at room temperature without stabilizers (Tsunekama et al. 2003; Pitcher et al. 2005).

Nanocrystalline zirconia can be obtained from hydrous zirconia, and the crystallinity depends on the synthesis conditions as alkali and its concentration, the rate of addition during the reaction, pH, and temperature. Some other parameters need to be taken into account, such as the presence of other anions/cations, the use of surfactants and post-treatment processes as well as the washing and drying (Srinivasan and Davis 1992; Srinivasan et al. 1993; Chuah and Jaenicke 1997; Chuah et al. 1998; Dell'Agli et al. 1999; Dell'Agli et al. 2008; Matsui and Ohgai 2002; Jiao et al. 2003; Stenina et al. 2008).

Many authors consider hydrous zirconia and zirconium hydroxide as synonyms. Huang et al. (2001), however, evaluated the two substances and proposed a structure for hydrous zirconia consisting of a cluster of 16 zirconium cations, 20 non-bridging hydroxo groups, 22 bridging hydroxo groups (may be understood as Zr-O-Zr bonds), and 20 coordinated water molecules. According to authors (Huang et al. 2001), hydrous zirconia and zirconium hydroxide are different materials with mass losses after calcination of 21.5 and 32.2%, respectively. Besides that, they have different solubility in acidic medium and only zirconium hydroxide is soluble in aqueous HNO₃. In addition, it is used as the precursor material for the production of zirconia, hydrous zirconia also finds application as a catalyst in various chemical reactions of commercial interest (Jaenicke et al. 2008; Song et al. 2011), as well as for removal of contaminants present in aqueous media (Chitrakar et al. 2006; Pan et al. 2013).

Hydrous zirconia can be produced by several methods, including forced hydrolysis in acid medium (Marković and Milonjić 2006), sol-gel followed by refluxing (Štefanić et al. 2000; Aguila et al. 2006) or ultrasound (Gubanova et al. 2015), reverse microemulsion (Tai et al. 2004), and polymeric precursor (Castro et al. 2008). However, the precipitation from ZrCl₄, ZrOCl₂·8H₂O or ZrO(NO₃)₂ solutions with alkalis followed by refluxing or hydrothermal treatment of the powders is the most widely used method reported throughout the literature (Chuah et al. 1998; Dell'Agli et al. 2008; Stenina et al. 2008; Wang et al. 2007).

First reported by Clearfield (1964), the production of nanocrystalline hydrous zirconia, cubic or tetragonal, with crystallites size from 2.0 to 2.5 nm presented similar structure to the calcined oxide. The author considered the hydrous zirconia as ZrO₂ with many hydroxyl groups and molecular water adsorbed on the powder surface.

Zirconia was first obtained from ZrW₂O₈ when trying to remove WO₃ which had not reacted in the synthesis of ZrW₂O₈ (Perotoni 2000). Although at first it was believed that the material obtained was amorphous, Somavilla et al. (2011) presented experimental evidence that the reaction between NaOH solution and ZrW₂O₈ resulted in hydrous tetragonal zirconia (ZrO₂·2H₂O) nanoparticles with crystallite size less than 2 nm. Therefore, more studies need to be done to find out how the experimental parameters affect the hydrous zirconia obtained from ZrW₂O₈ and also the mechanism of hydrolysis of the zirconium tungstate, which is an insoluble precursor in water, to prepare zirconia.

α-ZrW₂O₈ is a bimetallic oxide synthesized from ZrO₂ and WO₃ at temperatures near to 1200 °C and rapidly cooled to retain metastable cubic phase at room temperature (Vural 2011; Lind 2012). The crystal structure of α-ZrW₂O₈ can be described as a three-dimensional arrangement of corner-sharing ZrO₆ octahedra and WO₄ tetrahedra. In each WO₄ tetrahedron, one of the oxygen atoms is not bonded to the neighboring zirconium (terminal oxygen), providing the ZrW₂O₈ structure with a high degree of flexibility and isotropic negative thermal expansion ($-8.7 \times 10^{-6} \text{ K}^{-1}$) over a wide temperature range (from -272.7 to 777 °C) (Lind 2012; Chaplot 2005).

Accordingly, this study aimed to investigate the production of hydrous nanocrystalline zirconia from ZrW₂O₈, with different synthesis conditions to elucidate the influence of NaOH concentration, reaction time and temperature. In fact, it is expected that not only the hydrous zirconia, but also the zirconia obtained by this method, can exhibit very particular characteristics (as specific area, porosity, and crystalline structure) due to the precursor (Deshmane and Adewuyi 2012), thus having an impact on possible applications.

Materials and methods

Synthesis of zirconia

All experiments were carried out at the same proportion of α-ZrW₂O₈ (Wah Chang Co., Albany - OR, USA) to

NaOH solution, namely 0.2 g of zirconium tungstate for 100 mL of solution. The effect of NaOH (Vetec, 97%) concentration on synthesis product was evaluated using 1, 2, 3, 4 and 5 mol L⁻¹ at 5 h at 80 °C. Reaction time impact was evaluated at 5 and 10 min and 1, 3, 5, 8 and 10 h at 80 °C using a 1 mol L⁻¹ NaOH solution. The effect of reaction temperature was assessed at 60, 70, 80, 90 and 100 °C using a 2 mol L⁻¹ NaOH solution for 5 h. All experiments were carried out using Teflon flasks under magnetic bar stirring. The precursor (zirconium tungstate) was added only after the solution had reached the prescribed temperature. After each reaction, the resulting suspension was filtered using a membrane with a pore size less than 0.45 μm and the retained products were thoroughly washed with deionized water until neutral pH. After dried at 120 °C for 12 h, the product was stored at room conditions for further characterization. Over 85% of the zirconium present in the original zirconium tungstate is recovered in the filtered sample.

Characterization

The sodium content was estimated by semiquantitative EDS analysis on a Shimadzu SSX-550 scanning electron microscope, working at 15 kV, with an acquisition time of 15 min and a working distance of 16 mm. The tungsten content was determined by EDXRF, using the Fundamental Parameters method, in a Shimadzu EDX-7000 spectrometer operating with a rhodium tube at 50 kV, with an acquisition time of 100 s.

Samples were also characterized by XRD using a Shimadzu LABX XRD-6000 diffractometer operating with CuKα radiation ($\lambda = 0.15418$ nm). The measurements were carried out with a step size of 0.05°, integration time of 2 s, 1° divergence and scattering slits, 0.15 mm receiving slit and sample rotating at 10 rpm. Crystallite size was calculated according to the procedure described by Delhez et al. (1993), subtracting the instrumental contribution to peak broadening and taking into account the most intense diffraction peak ($2\theta \sim 30.2^\circ$) fitted by a pseudo-Voigt profile function.

Crystallite size and some interplanar distances for the sample synthesized with NaOH 1 mol L⁻¹, at 80 °C for 1 h, were also evaluated by TEM in an FEI TECNAI 20 microscope operating at 200 kV. For this analysis, the sample was previously dispersed in acetonitrile using an ultrasound bath, and a thin film of this suspension was deposited on a copper grid and covered with carbon.

Phase identification was carried out with the aid of Raman spectroscopy with an HORIBA LabRAM HR Evolution 800 spectrophotometer equipped with a He-Ne laser ($\lambda = 632.8$ nm). Raman spectra were acquired from 100 to 1000 cm⁻¹, with 10 accumulations of 100 s each, using a 600 lines mm⁻¹ diffraction grating, 50 μm entrance slit, and a × 50 microscope objective.

Further vibrational spectroscopy analysis was performed using diffuse reflectance Fourier-transform infrared spectroscopy (DRIFTS) on a PERKIN-ELMER Spectrum 400 spectrometer. The spectra were collected from 4000 to 450 cm⁻¹, with a resolution of 4 cm⁻¹ and 64 scans. Before this analysis, samples were dried for 24 h at 120 °C to remove residual moisture.

Simultaneous TG and DSC measurements were carried out on an NETZSCH STA 449 F3. The evolved gases were analyzed by mass spectroscopy on an NETZSCH QMS 403 mass spectrometer. For this, around 15 mg powdered samples were packed inside Pt crucibles around 15 mg, evacuated at 80 °C for 1 h and then heated to 1000 °C at 10 °C min⁻¹ using Ar (40 mL min⁻¹). Water ($m/z = 18$) and CO₂ ($m/z = 44$) content in the evolved gases were deconvoluted in individual contributions using Gaussian fits (see Fig. S3 in Supplementary Information) (Wang et al. 2007).

Zr and W chemical distribution, as well as particle size and morphology analysis, were carried out using a field emission gun SEM TESCAN Mira3 LM microscope operating at 15 kV. Before analysis, ZrW₂O₈ was dispersed in water and ZrO₂ in an HCl solution (0.01 mol L⁻¹), sonicated during 4 min, and then deposited on an aluminum sample holder, let dry at room conditions and finally recovered with gold. Additionally, mapping images of the elements Zr and W, corresponding to an area of 1.2 mm² on the samples, were performed using X-ray microfluorescence in a BRUKER M4 Tornado spectrometer operating with a rhodium tube at 50 kV and 600 μA.

The specific area was determined by analysis of the isotherm of adsorption of nitrogen at 77 K on an MICROMERITICS Gemini III 2375 analyzer. Data analysis was performed according to BJH method (Barrett et al. 1951). The cross section area of nitrogen used in the calculations was 0.162 nm² (Sing et al. 1985). Pore width was estimated considering that the nitrogen monolayer thickness was equivalent to that proposed by Halsey (Rouquerol et al. 2014). The presence of micropores in the samples was evaluated by the empirical method suggested by Sing (Sing and Williams

2005), known as α_S -plot, taking ZrW_2O_8 as the reference. This approach allowed the determination of the external surface areas (a_{EXT}) of the samples in the multistep region (Marczewski 2002).

The true density (ρ) of ZrW_2O_8 and the samples synthesized using different reaction times (5 min, 5 and 10 h) with NaOH 1 mol L⁻¹ at 80 °C was evaluated by He pycnometry on an MICROMERITICS AccuPyc II 1340 gas pycnometer. The samples were kept in a vacuum at ambient temperature for at least 10 h before specific area and density measurements. Particle sizes (d_{BET}) were estimated as $d_{BET} = 6/\rho a_{BET}$ (Rouquerol et al. 2014).

Results

Elemental analysis

The samples, regardless synthesis conditions, are composed mainly of Zr and O. Furthermore, except for samples produced with NaOH 1 mol L⁻¹ to 80 °C for

5 min to 1 h, all others samples have sodium as an impurity (Table 1). Tungsten content in the samples was dependent on synthesis conditions. The W concentration tends to decrease with increasing reaction time and temperature, and also with NaOH concentrations higher than 1 mol L⁻¹ remaining, however, approximately constant for NaOH concentrations exceeding 2 mol L⁻¹.

The EDS mapping images of the 5 min sample (Fig. 1a, b) showed only some particles rich in tungsten and poor in zirconium. However, a homogeneous distribution of these elements was observed in the rest of the material. A similar result was obtained in mapping images taken by X-ray microfluorescence (Fig. S1a). The compositional maps for samples obtained after 5 (Fig. 1c, d) and 10 h of reaction time (Fig. S1b) exhibit a homogeneous distribution of tungsten throughout the material. In a few cases (for instance, the sample produced for 5 h with NaOH 1 mol L⁻¹ at 80 °C) some smaller agglomerates showed no evidence at all of tungsten in their composition (Fig. 1d), as confirmed by EDS spectrum of this part of the sample.

Table 1 Semiquantitative tungsten and sodium content, XRD crystallite size results and Lorentzian fraction in the pseudo-Voigt peak profile (η)

Experimental condition	Tungsten (atom%)	Sodium (atom%)	XRD crystallite size (nm)	η (dimensionless)
NaOH concentration effect (for 5 h at 80 °C)				
1 mol L ⁻¹	0.36	0.73	2	1.11
2 mol L ⁻¹	0.21	1.49	2	1.04
3 mol L ⁻¹	0.20	1.28	2	1.05
4 mol L ⁻¹	0.14	1.36	2	0.97
5 mol L ⁻¹	0.19	1.18	2	1.01
Synthesis reaction time effect (with NaOH 1 mol L ⁻¹ at 80 °C)				
5 min	2.85	–	1	1.11
10 min	1.10	–	1	1.12
1 h	0.74	–	1	1.17
3 h	0.68	1.18	1	1.29
5 h	0.36	0.73	2	1.11
8 h	0.27	1.31	3	1.00
10 h	0.25	1.13	3	1.00
Synthesis reaction temperature effect (with NaOH 2 mol L ⁻¹ for 5 h)				
60 °C	0.67	0.97	1	1.06
70 °C	0.38	0.97	1	1.28
80 °C	0.21	1.49	2	1.04
90 °C	0.17	1.88	3	0.91
100 °C	0.09	1.62	3	0.87

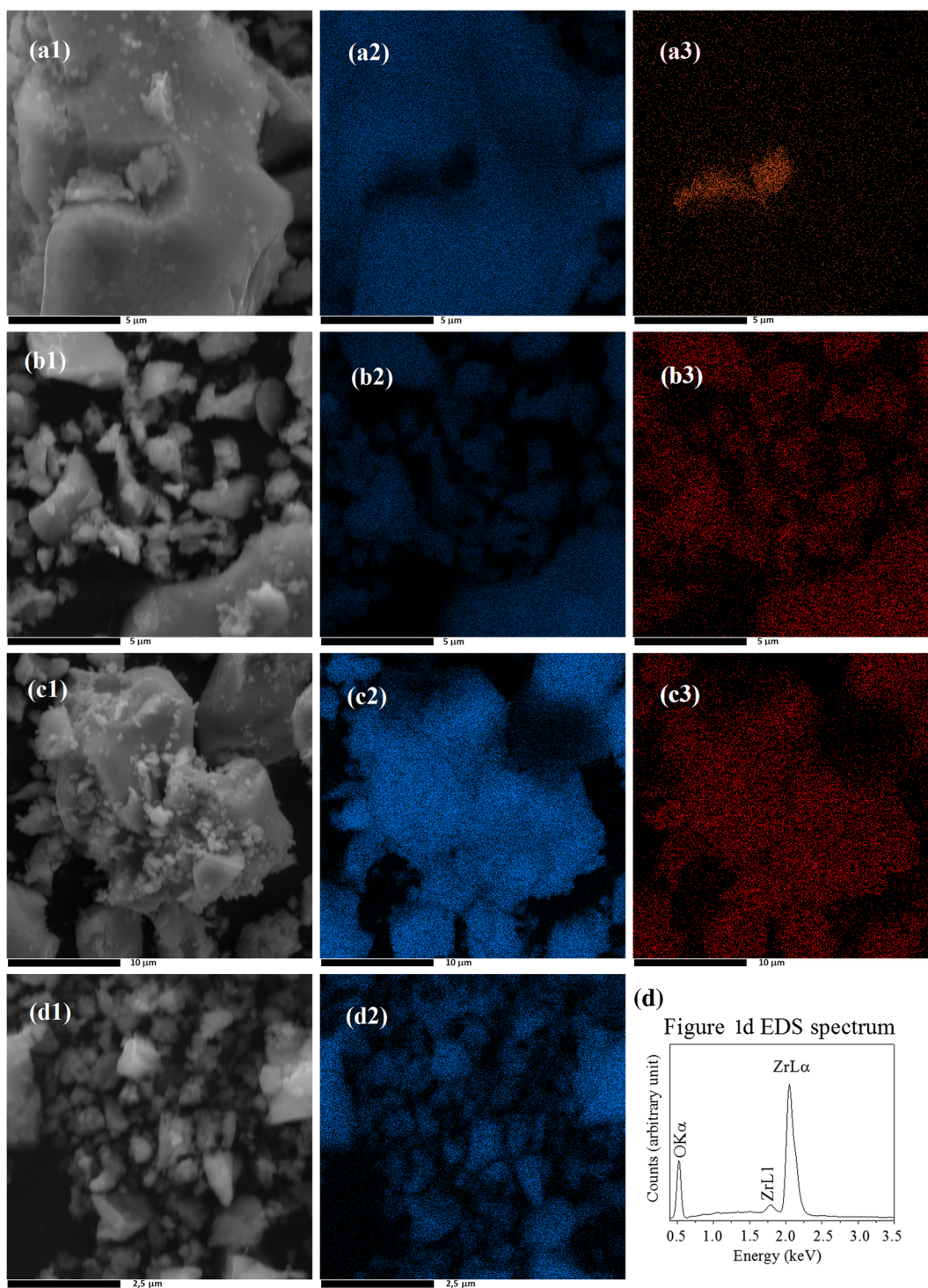


Fig. 1 Mapping images of the samples synthesized for (a, b) 5 min and (c, d) 5 h with NaOH 1 mol L⁻¹ at 80 °C. (1) scanning electron micrograph; (2) zirconium; (3) tungsten

X-ray diffraction

The X-ray diffraction (XRD) in Fig. 2a showed the presence of crystalline peaks characteristic of WO_3 (ICSD 1620) and a few Bragg peaks that might be assigned to monoclinic (ICSD 41572) as well as tetragonal/cubic zirconia (ICSD 97004/89429). This observation agrees with the existence of some particles free of zirconium according to EDS mapping (Fig. 1a). However, the WO_3 Bragg peaks disappear in just 10 min of synthesis, indicating that the residual oxide must have been solubilized in the highly alkaline medium forming tungstate ions (WO_4^{2-}). Low-intensity Bragg peaks were also observed in the XRD pattern of ZrW_2O_8 (Fig. 2b), thus indicating that there is a small contamination of zirconia in the precursor material.

While the monoclinic zirconia peaks remain present in the XRD pattern of all samples, regardless the experimental parameters of the synthesis, the tetragonal/cubic zirconia Bragg peaks get better defined with increasing reaction time and temperature, with only minimal changes upon increasing NaOH concentration. These observations are also valid for the crystallite size derived from the most intense Bragg peak ($2\theta \sim 30.2^\circ$) (Table 1). Table 1 also shows the fraction of Lorentzian profile (η) obtained from the fitting to the Bragg peak at $\sim 30.2^\circ$. The analysis of samples produced with NaOH solutions other than 4 mol L^{-1} (for 5 h at 80°C), those synthesized by periods of time less than 8 h (with NaOH 1 mol L^{-1} at 80°C) and also those produced using temperatures below 90°C (with NaOH 2 mol L^{-1} for 5 h) yielded $\eta > 1$. A super-Lorentzian profile ($\eta > 1$) indicates a broad crystallite size distribution (Langford et al. 2000; Balzar and Popa 2002).

NaOH concentration did not seem to affect the product's crystallite size significantly. As synthesis time increased, the product's crystallite size also increased up to a maximum of 3 nm at 8 h, remaining essentially unchanged for 10 h of synthesis time (Table 1). Regarding the effect of temperature on the synthesis (Table 1), it was noted that the crystallite size also increased, possibly because of the formation of Zr-O-Zr bonds through condensation of hydroxyl groups and release of H_2O . For temperatures up to 80°C , the crystallite size distribution is multimodal (crystallites rearrangement in progress), while that above 80°C , the size remains constant (3 nm).

Transmission electron microscopy

Transmission electron microscopy (TEM) of the sample produced with NaOH 1 mol L^{-1} for 1 h at 80°C is shown in Fig. 3a. This analysis revealed micrometer size polycrystalline agglomerates as suggested by the electron diffraction pattern (Fig. 3b) consisting of crystallites smaller than 5 nm. The interplanar distance was calculated using the ImageJ software for the marked area in Fig. 3a and evaluated by the fast Fourier transform in Fig. 3c. The interplanar distance, 0.295 nm, is similar to the expected value for a scattering angle $2\theta = 30.3^\circ$, as obtained for this sample by XRD using $\text{CuK}\alpha$ radiation, and can be assigned to either tetragonal or cubic zirconia.

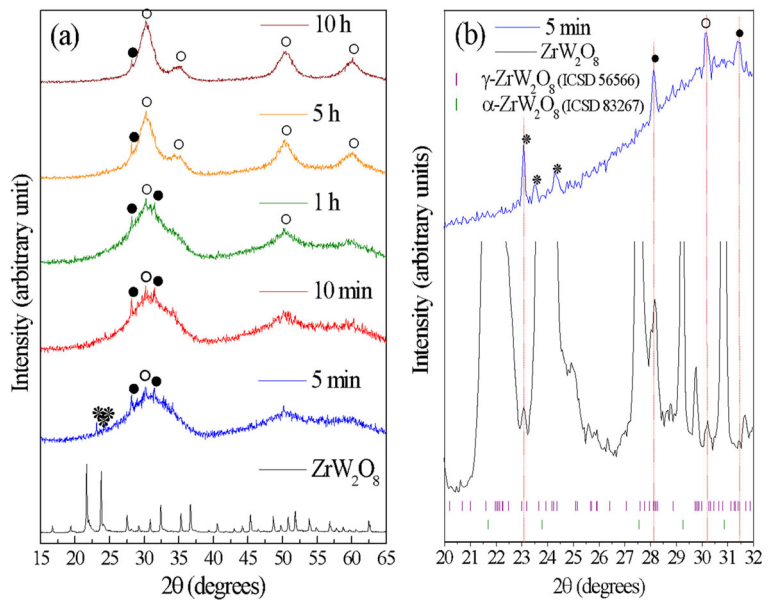
Raman spectroscopy

Figure 4 shows the Raman spectra of some samples produced under different experimental conditions (Raman spectra for the entire set of samples are in Supplementary Information - Fig. S2). Raman spectroscopy allowed unambiguous identification of the tetragonal and cubic phases of zirconia in the synthesized samples, which was not possible by XRD.

Regardless of the experimental condition, the Raman spectra of all the samples exhibited a broad peak between 500 and 600 cm^{-1} , which can be assigned to cubic zirconia (Tahir et al. 2007). Tetragonal zirconia can be detected in samples produced at 90 and 100°C (for 5 h with NaOH 2 mol L^{-1}) (Fig. 4b), as well as in those produced with 3 and 4 mol L^{-1} NaOH solutions (at 80°C for 5 h) (Fig. 4c). Indeed, the Raman spectra of these samples show peaks at 143 cm^{-1} , assigned to the angular deformation of the O-Zr-O and Zr-O-Zr bonds, and $\sim 260 \text{ cm}^{-1}$, characteristic of Zr-O bond stretching (Tang and Zheng 2004).

Characteristic peaks of monoclinic zirconia (~ 175 and $\sim 190 \text{ cm}^{-1}$) were present in the Raman spectra of all synthesized samples (Kim and Hamaguchi 1997; Daramola et al. 2010). Those peaks were more clearly identifiable in the spectra of samples obtained at higher temperatures and NaOH concentration, as well as longer reaction time, thus indicating a better crystallization of the monoclinic phase in these materials (Fig. S2). The Raman spectrum of the sample produced for 5 min at 80°C , with NaOH 1 mol L^{-1} (Fig. 4a) exhibited a peak around 802 cm^{-1} which can be attributed to monoclinic

Fig. 2 **a** XRD patterns of samples synthesized with NaOH 1 mol L⁻¹ at 80 °C, for different reaction times, and the precursor ZrW₂O₈. **b** Evidence of the presence of tungsten oxide (* = ICSD 1620), monoclinic (● = ICSD 41572) and tetragonal/cubic zirconia (○ = ICSD 97004/89429) in ZrW₂O₈ and in the sample synthesized for 5 min; the small ticks at the bottom mark the expected positions of the Bragg peaks from γ-ZrW₂O₈ and α-ZrW₂O₈



tungsten oxide (Ross-Medgaarden and Wachs 2007) in good agreement with previously described XRD results.

Infrared spectroscopy

All samples exhibited a diffuse reflectance infrared Fourier transform spectroscopy (DRIFTS) spectrum similar to that shown in Fig. 5. Accordingly, regardless the synthesis conditions and the drying step at 120 °C

before the DRIFTS analysis, samples still have physically and chemically bonded water as signaled by the broad infrared bands at ~3360 cm⁻¹ and ~1637 cm⁻¹. However, the infrared bands assigned to hydroxyl (between 4000 and 3500 cm⁻¹) and carbonate (between 1800 and 800 cm⁻¹) vibrations (Bachiller-Baeza et al. 1998) experienced changes depending on the experimental conditions used in the synthesis (Table 2).

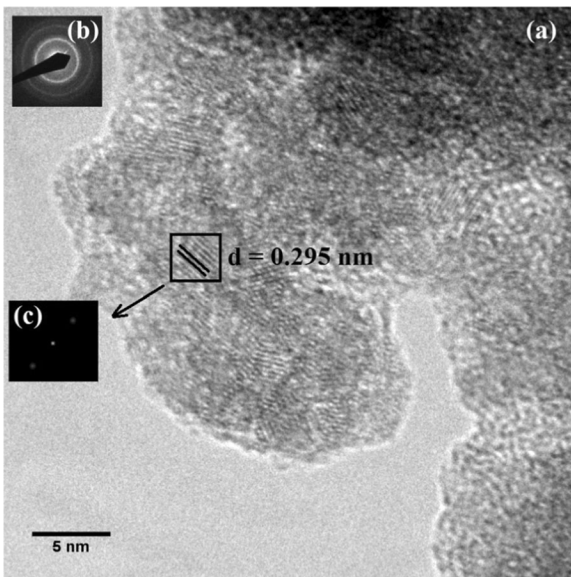


Fig. 3 **a** High-resolution TEM of the sample produced with NaOH 1 mol L⁻¹, for 1 h at 80 °C; **b** electron diffraction pattern; **c** fast Fourier transform of the demarcated region

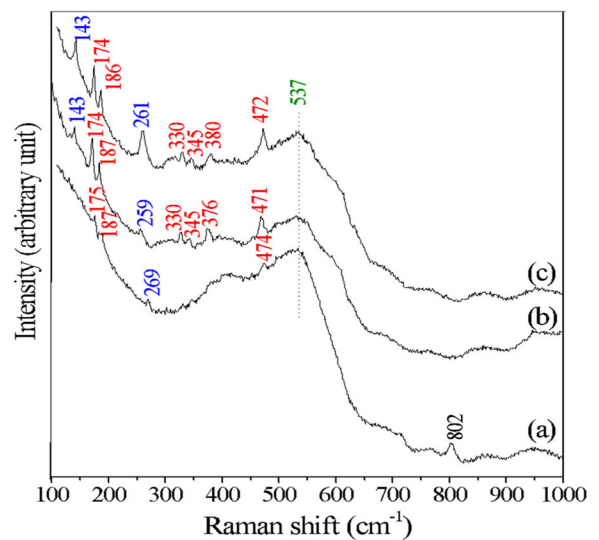


Fig. 4 Raman spectra of samples produced using different synthesis conditions. **a** NaOH 1 mol L⁻¹, 5 min, 80 °C; **b** NaOH 2 mol L⁻¹, 5 h, 100 °C; **c** NaOH 3 mol L⁻¹, 5 h, 80 °C. Blue = *t*-ZrO₂; red = *m*-ZrO₂; green = *c*-ZrO₂; black = *m*-WO₃

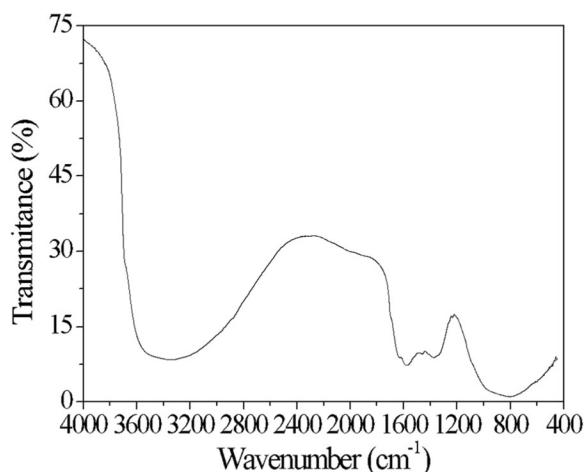


Fig. 5 DRIFTS spectrum of the sample synthesized with NaOH 1 mol L^{-1} for 5 h at $80 \text{ }^\circ\text{C}$

Simultaneous thermal analysis–mass spectrometry

When subjected to thermogravimetric analysis (TG), all samples exhibited a significant weight loss during the pre-treatment under a vacuum at $80 \text{ }^\circ\text{C}$. This weight loss is due to water and CO_2 weakly bonded to the material ($12.3 \pm 2.2\%$), and is followed by a second weight loss by heating to $1000 \text{ }^\circ\text{C}$ ($7.6 \pm 1.0\%$). The average total weight loss was $19.8 \pm 2.3\%$, and sample masses remained constant above $850 \text{ }^\circ\text{C}$. Identification of chemical species in the evolved gas was aided by quadrupole mass spectrometry (QMS, see Supplementary Information Fig. S3 and Tables S1–S3).

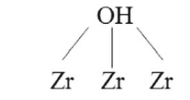
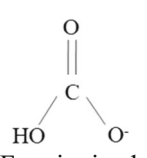
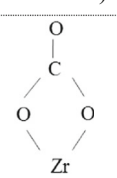
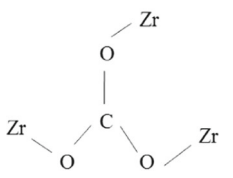
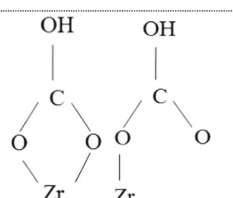
With regard to the effect of NaOH concentration on the synthesis products, the sample produced with NaOH 5 mol L^{-1} and dried at $120 \text{ }^\circ\text{C}$ exhibits stronger Raman peaks characteristic of monoclinic zirconia as compared to samples produced with lower NaOH concentrations (Fig. S2a). This sample underwent a significant water loss (21%) at temperatures above $400 \text{ }^\circ\text{C}$, possibly because water adsorbs in greater amounts in monoclinic zirconia, as seen in hydration modeling studies (Piskorz et al. 2011; Piskorz et al. 2012). This sample also has fewer types of carbonate species present on its surface (Table 2), with little evidence of polydentate carbonate, for example. Perhaps this could explain the observation that the temperature range over which CO_2 loss is observed in the mass spectrometric analysis is narrower (between 245 and $690 \text{ }^\circ\text{C}$) than in samples produced with lower NaOH concentrations (between 224 and $826 \text{ }^\circ\text{C}$ and between 185 and $675 \text{ }^\circ\text{C}$ for the samples produced with NaOH 1 and 2 mol L^{-1} , respectively) (Table S1).

DRIFTS results (Table 2) suggest that samples produced at increasing synthesis temperature have different types of carbonate species adsorbed, including polydentate carbonates, which are only eliminated at higher temperatures during thermogravimetric analysis. Accordingly, the sample produced at $60 \text{ }^\circ\text{C}$ showed a significant CO_2 loss (47%) below $250 \text{ }^\circ\text{C}$, which might be attributed to the decomposition of bicarbonate species. On the other hand, the sample produced at $100 \text{ }^\circ\text{C}$ exhibited a greater loss of CO_2 above $500 \text{ }^\circ\text{C}$ (45% , compared to 10 and 13% for the samples produced at 60 and $80 \text{ }^\circ\text{C}$, respectively) (see Table S2). This last sample showed the strongest Raman peaks of tetragonal zirconia (Fig. S2c) which, according to literature, may favor the formation of surface polydentate carbonates (Bachiller-Baeza et al. 1998). With regard to water loss under heating, samples have exhibited greater weight loss contributions at higher temperatures (292 and $337 \text{ }^\circ\text{C}$ for samples produced at 60 and $100 \text{ }^\circ\text{C}$, respectively) (Table S2). This indicates that water is increasingly strongly adsorbed as the temperature of synthesis increases.

In results from DRIFTS analysis (Table 2), all samples, regardless of the reaction time, showed bands corresponding to bicarbonate species that are eliminated at low temperatures ($300 \text{ }^\circ\text{C}$). However, from 5 h of reaction on, samples began to show evidence of the presence of polydentate carbonate which, according to the literature, have higher thermal stability (Bachiller-Baeza et al. 1998; Köck et al. 2013). Therefore, for samples obtained with reaction times of 5 h or greater, CO_2 losses came to have significant contributions above $500 \text{ }^\circ\text{C}$ (around 38%), which can be attributed to the elimination of polydentate carbonates (Table S3). Regarding water loss, as the synthesis time increased the greatest weight loss contributions also occurs at higher temperatures, from 200 to $270 \text{ }^\circ\text{C}$ (1 h) to $338 \text{ }^\circ\text{C}$ (3 h) and to $385 \text{ }^\circ\text{C}$ (for 10 h reaction) (Table S3). This suggests that with increasing reaction time, a more condensed structure (with Zr-O-Zr substituting for Zr-OH bonds) leads to a material with higher thermal stability.

Samples were also characterized by differential scanning calorimetry (DSC) and, after thermal treatment in an inert atmosphere up to $1000 \text{ }^\circ\text{C}$, were again analyzed by Raman spectroscopy (Table 3). The loss of physically and chemically bonded water and the elimination of CO_2 (by decomposition of bicarbonate or CO_2 interacting with the surface by hydrogen bonds) (Wang et al. 2007) is accompanied by an endothermic event

Table 2 Band assignments for the DRIFTS spectra of zirconia samples

Wavenumber (cm ⁻¹)	Assignment	Influence of synthesis conditions
3695	 <p>Triply coordinated hydroxyl (Bachiller-Baeza et al. 1998)</p>	The band has the same intensity independent of the concentration of NaOH used for 5 h reactions at 80 °C. However, for a given concentration of NaOH, an increase in time or temperature enhances this band, which becomes better defined, suggesting that these factors affect the formation of Zr-OH bonds with the elimination of water.
1700	 <p>Free ionized bicarbonate (Pokrovski et al. 2001)</p>	In experiments varying NaOH concentration, this band was observed only in the products of reaction with NaOH 1 mol L ⁻¹ . This behavior can be attributed to the fact that a larger amount of hydroxyl groups in the medium, with increasing NaOH concentration, disfavors the presence of ionized bicarbonate. Regarding temperature, the band was only evident in the sample produced at 60 °C. This band was present in all samples produced at varying reaction time.
~1570-1370	 <p>Bidentate carbonate (Bachiller-Baeza et al. 1998; Köck et al. 2013)</p>	These bands are the only common to all samples, regardless of the experimental condition, and are related to the presence of Zr ⁴⁺ -O ²⁻ sites of high basicity (Daramola et al., 2010).
~1460-1420	 <p>Polydentate carbonate (Pokrovski et al. 2001)</p>	These carbonate bands can provide information about the system crystallization stage: using NaOH 5 mol L ⁻¹ these bands are missing, possibly because in this situation the high system crystallization rate, due to a significant amount of hydroxyl available in the medium, reduces the sites available for carbonate adsorption. On the other hand, the approximation of cationic centers promoted at temperatures above 80 °C and from 5 h of reaction time favors the formation of this kind of polydentate species.
~1236, 1016, and 794	 <p>Bicarbonate (Bachiller-Baeza et al. 1998; Palmer and Eldik, Silverstein et al. 1991)</p>	These bands are present in samples that have more terminal hydroxyl groups that are linked to coordinately unsaturated zirconium ions (Morterra and Orto, 1990), like those produced with NaOH 1 and 3 mol L ⁻¹ (for 5 h at 80 °C), 60 °C (with NaOH 2 mol L ⁻¹ for 5 h), and in all those samples produced with different reaction times (with NaOH 1 mol L ⁻¹ at 80 °C).

extending from room temperature to about 400 °C. Further exothermic events associated with structural modifications in the samples upon heating are summarized in Table 3.

Samples produced in 5 min, 10 min, 1 h and 8 h (with NaOH 1 mol L⁻¹ at 80 °C), and at 60 and 100 °C (with NaOH 2 mol L⁻¹ for 5 h) (Table 3), exhibited an exothermic peak with weight loss between 430 and 590 °C.

This exothermic peak may be related to the elimination of hydroxyl groups (and associated CO_2) by condensation reactions. The temperature of this thermal event, as well as the enthalpy and activation energy, is dependent on the synthesis conditions (Table 3). In fact, the sample produced with NaOH 5 mol L^{-1} (for 5 h at 80°C) barely exhibits this exothermic peak.

At temperatures above 500°C , samples lose CO_2 originally present in the form of surface bidentate and polydentate carbonates (Wang et al. 2007). A more complex behavior is observed above 850°C (Table 3). Indeed, while some samples exhibit exothermic abrupt events at 950°C , other shown less abrupt events between 890 and 950°C , all without any significant accompanying mass loss and possibly associated to phase transitions, judging by the corresponding Raman spectra before and after heating (Table 3). In contrast, most of the samples showed no distinct peaks at higher temperatures.

According to the literature, the tetragonal-monoclinic phase transition in nanocrystalline zirconia may occur above 500°C . This non-equilibrium phase transition has, therefore, a kinetic character (Blesa et al. 1985), so that the presence of impurities and different phases, crystallite size and even the thermal history of the sample may interfere with the phase transition. Therefore, it was not possible to establish a clear relationship between the observation of the sharp exothermic peak at 950°C and the synthesis conditions. Anyway, there was a tendency to the predominance of the tetragonal phase in samples produced with higher concentrations of NaOH and lower temperatures and synthesis time. The crystallite size for this phase, calculated according to Djuraro et al. (2000) and shown in Table 3, revealed that these samples are nanocrystalline even after heating to 1000°C in an inert atmosphere.

Scanning electron microscopy

Scanning electron microscopy (SEM) images of the zirconia samples exhibit a heterogeneous distribution of particle size and agglomerates (only micrographs related to the effect of time are shown) (Fig. 6b, c). Overall, the images show zirconia particles and micrometer-sized agglomerates of nanoscale particles, with corners and irregular shapes resembling the zirconium tungstate precursor (Fig. 6a).

A common feature for all the samples is that, contrarily to the precursor ZrW_2O_8 , the surface of particles and agglomerates, while seemingly smooth and homogeneous at low magnifications, is composed of nearly spherical nanoparticles smaller than 20 nm ($500,000\times$).

Surface area, porosity, and density

Nitrogen adsorption isotherms at 77 K and pore size distribution are summarized in Figs. 7 and 8. Results for the specific area calculated according to the Brunauer, Emmett, and Teller (BET) method, the outer area and porosity obtained from the α_S -plot, total pore volume obtained by the Barrett, Joyner and Halenda (BJH) method, the true density and particle size calculated from the surface area and density are summarized in Table 4. The α_S -plots were constructed taking into account the parent zirconium tungstate as a reference (Fig. S4).

The specific area and total pore volume experienced a significant increase in samples of zirconia produced at different reaction times, as compared to the precursor (Table 4). Zirconium tungstate exhibits a type II adsorption isotherm (Fig. 7a), according to the classification of the International Union of Pure and Applied Chemistry – IUPAC (Sing et al. 1985), characteristics of non-porous or macroporous material (pores greater than 50 nm) materials. Given that zirconium tungstate presents a small pore volume and the fact that the adsorption isotherm grows faster at relative pressures near unity, it can be inferred that ZrW_2O_8 is macroporous (Sing et al. 1985). This was further corroborated by the pore size distribution (Fig. 8a), for which the largest pore volume is close to 50 nm .

After only 5 min of synthesis, the product already exhibits a behavior dissimilar to that of the precursor. All zirconia samples evaluated have type IV adsorption isotherms (Fig. 7b-d) with the hysteresis loops characteristic of mesoporous materials (pore size between 2 and 50 nm) (Sing et al. 1985). In the case of the sample obtained after 5 min of synthesis, the adsorption and desorption curves in the hysteresis region are almost parallel horizontally, and there is no adsorption saturation for high pressures. This behavior is similar to that of type H4 hysteresis loop, typical of narrow slit-shaped pores within the micropore range, i.e., less than 2 nm (Sing et al. 1985; Rouquerol et al. 2014), a finding that is in agreement with pore volume distribution (Fig. 8b). For the

Table 3 Exothermic events observed in DSC curves for samples synthesized under different experimental conditions. Monoclinic, tetragonal, and cubic zirconia are represented by *m*, *t*, and *c*, respectively

Experimental condition	Structural change			Crystalline structure		
	<i>T_p</i> (°C)	Δ <i>H</i> (kJ mol ⁻¹)	<i>E_a</i> (kJ mol ⁻¹)	With mass loss	Without mass loss	Crystallite size (nm)*
NaOH concentration effect (for 5 h at 80 °C)						
1 mol L ⁻¹	—	—	—	n.p.	m, c	m, t ~15
2 mol L ⁻¹	—	—	—	950 (s)	c	m —
5 mol L ⁻¹	450–550	n.d.	n.d.	890 and 950 (m)	m, c	m, t (higher amount) 10–15
Synthesis temperature effect (with NaOH 2 mol L ⁻¹ for 5 h)						
60 °C	458	-11.8	211	n.p.	m, c	t < 5
80 °C	—	—	—	950 (s)	c	m —
100 °C	581	-6.71	247	n.p.	m, t, c	m, t (traces) n.d.
Reaction synthesis time (with NaOH 1 mol L ⁻¹ at 80 °C)						
5 min	444	-19.8	207	n.p.	m, t, c	t < 5
10 min	443	-12.7	206	950 (s)	m, c	n.d. n.d.
1 h	437	-12.5	204	950 (s)	c	n.d. n.d.
3 h	—	—	—	n.p.	m, t, c	t 5–10
5 h	—	—	—	n.p.	m, c	m, t ~15
8 h	456	-4.41	210	650 and 850 (m)	m, c	m n.d.
10 h	—	—	—	n.p.	m, c	m, t (lower amount) ~15

T_p = peak temperature

Δ*H* = enthalpy change considering a molar mass equal to 150 g mol⁻¹ (equivalent to ZrO(OH)₂·½H₂O, with a weight loss of 18%)

E_a = activation energy according to Redhead equation (Chuah et al., 1998)

n.p. = no defined peak; s = strong; m = moderate

*Tetragonal crystallite size after thermal treatment at 1000 °C in an argon atmosphere, calculated according to Djuraro et al. (2000)

n.d. = not determined

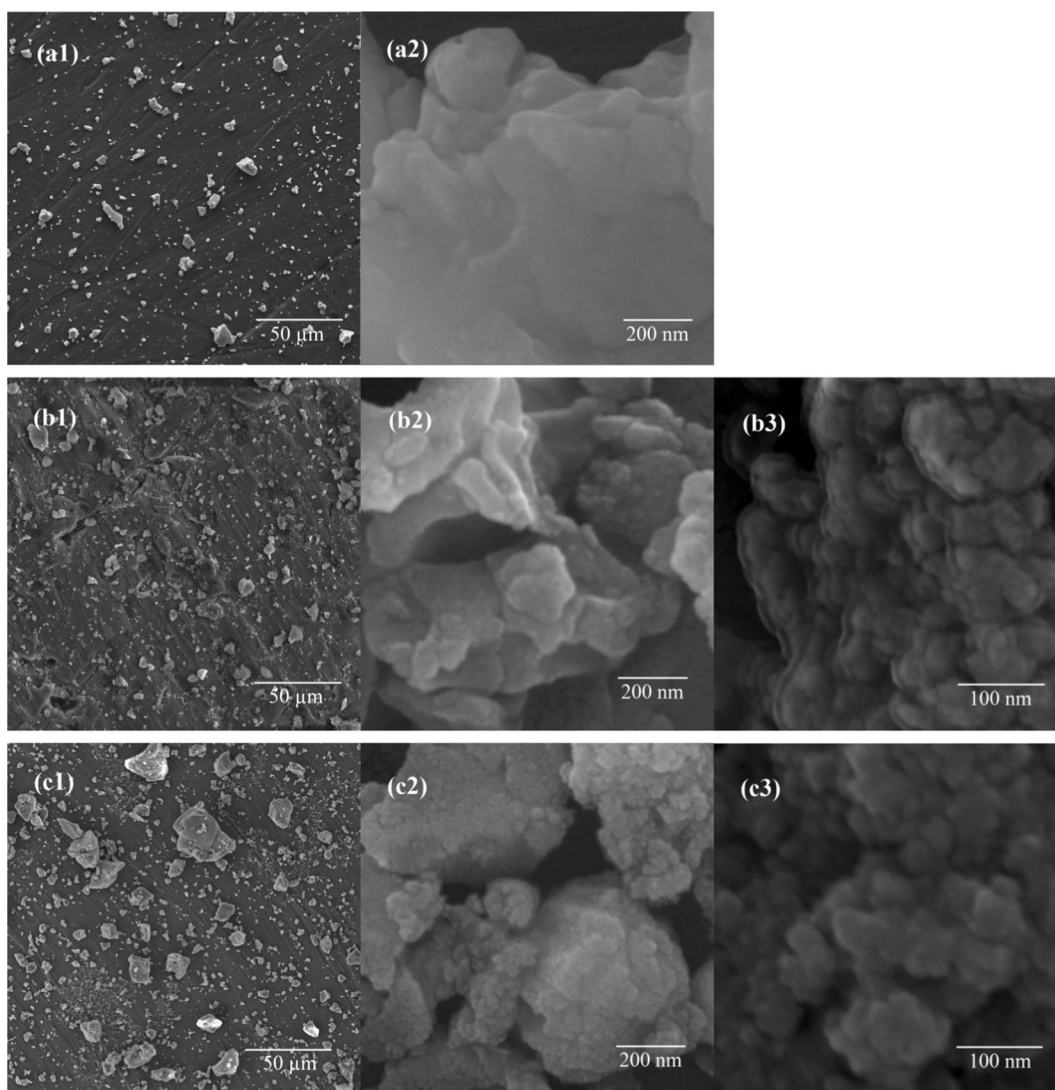


Fig. 6 SEM micrographs of a ZrW_2O_8 and samples synthesized for **b** 5 min, and **c** 10 h with NaOH 1 mol L^{-1} at 80°C ; magnifications: (1) $\times 1000$; (2) $\times 200,000$; (3) $\times 500,000$

sample obtained after 5 min of synthesis, the constant C is similar to that of the precursor (Table 4), suggesting that both samples have similar surfaces, in contrast to samples synthesized for 5 and 10 h.

The remaining zirconia samples subjected to N_2 adsorption analysis exhibited H2-type hysteresis loops, thus suggesting a complex porous structure formed by interconnected pore networks of different shapes and sizes, commonly observed in inorganic oxide gels and porous glasses (Sing et al. 1985; Rouquerol et al. 2014). Average pore size increased from 2.5 to 3 nm upon increasing reaction times from 5 to 10 h. There is no

indication of pores greater than 10 nm for any of these samples (Fig. 8b).

The zirconia samples exhibited specific areas (external and total) larger than that of parent ZrW_2O_8 . Furthermore, the primary particle size of the samples (about 5 nm) is almost three orders of magnitude lower than that of ZrW_2O_8 ($1.7 \mu\text{m}$). The true densities reported in Table 4 are lower than that for monoclinic (5.56 g cm^{-3}), tetragonal (6.10 g cm^{-3}) and cubic zirconia (5.83 to 6.20 g cm^{-3} , depending on the dopant) (Stevens 1986; Shukla and Seal 2005).

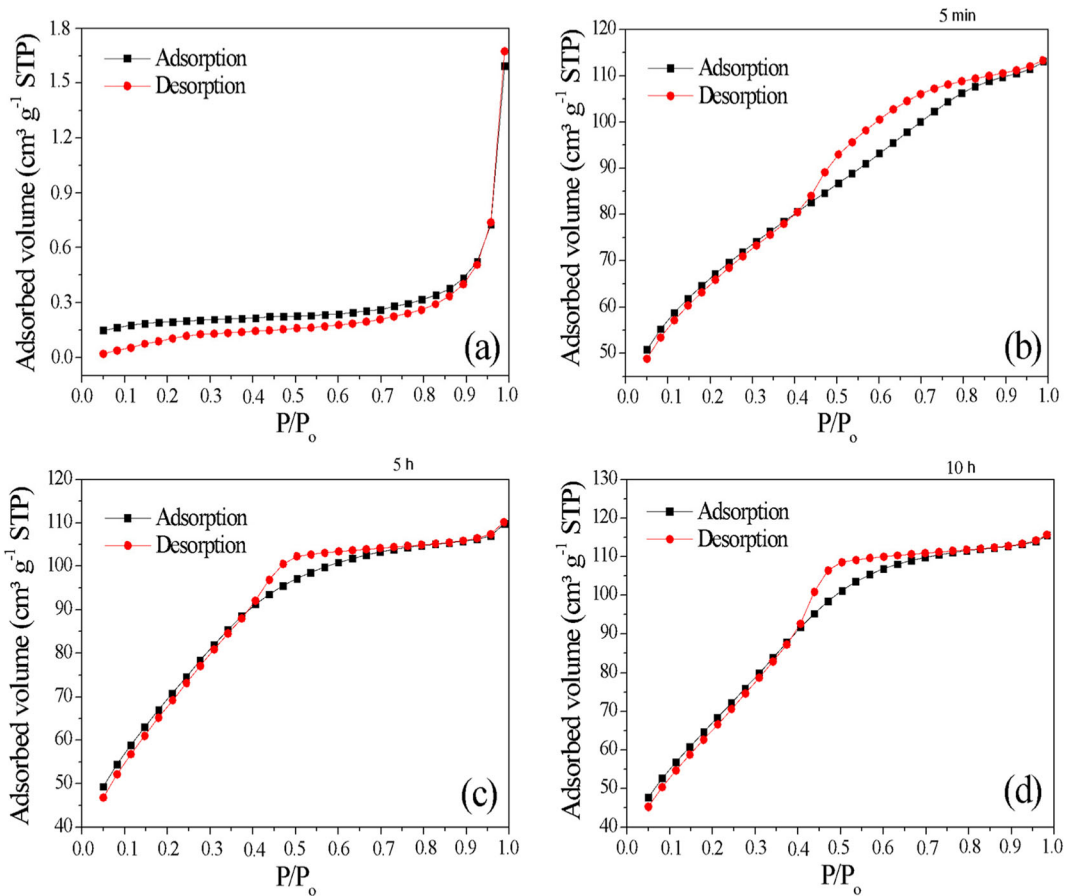


Fig. 7 Nitrogen adsorption-desorption isotherms at 77 K for **a** ZrW_2O_8 and zirconia samples synthesized with $NaOH$ 1 mol L^{-1} at $80\text{ }^\circ\text{C}$ for **b** 5 min, **c** 5 h, and **d** 10 h

Discussion

Preliminary studies suggested that synthesis of hydrous zirconia from ZrW_2O_8 resulted from selective leaching of WO_4 tetrahedra in alkaline medium (Perottoni 2000;

Somavilla et al. 2011). Accordingly, despite an increase of porosity, it was expected that the size and morphology of hydrous zirconia particles would remain similar to that of ZrW_2O_8 . Furthermore, the reaction was apparently slow and, therefore, the presence of residual

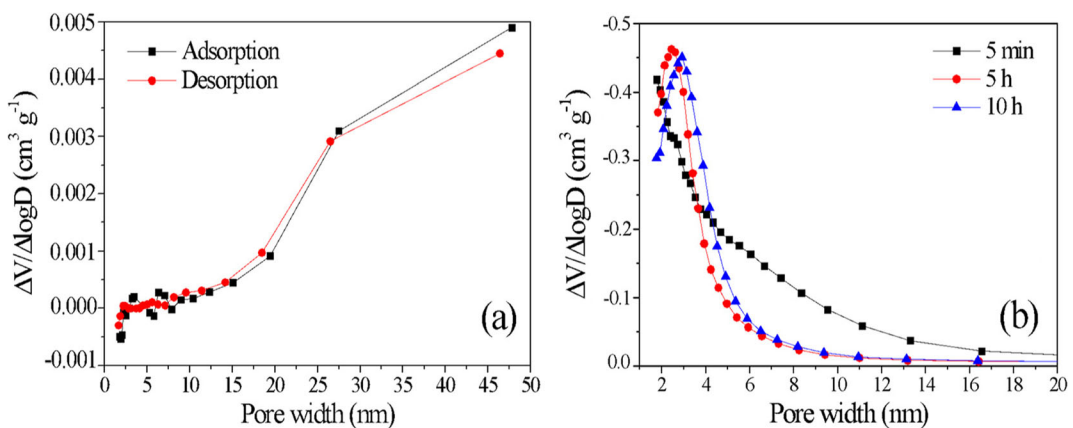


Fig. 8 Pore size distribution for **a** ZrW_2O_8 and **b** zirconia samples obtained after different synthesis times

Table 4 Specific area, porosity, density (ρ) and primary particle size (d_{BET}) obtained by different methods for ZrW_2O_8 and for hydrous zirconia samples synthesized for various reaction times with NaOH 1 mol L⁻¹ at 80 °C

Sample	BET			α_S -plot*				BJH		ρ (g cm ⁻³)	d_{BET} (nm)
	a_{BET} (m ² g ⁻¹)	V_m (cm ³ g ⁻¹)	C	$a_{ext-mier}$ (m ² g ⁻¹)	V_{micro} (cm ³ g ⁻¹)	$a_{ext-mes}$ (m ² g ⁻¹)	V_{total} (cm ³ g ⁻¹)	V_{total} (cm ³ g ⁻¹)			
ZrW_2O_8	0.710	0.163	130	n.d.	n.d.	n.d.	n.d.	0.0026	5.09	1660	
5 min	238	54.8	141	198	0.0147	1.60	0.169	0.175	5.09	4.94	
5 h	253	58.2	71.4	232	0.00158	2.43	0.161	0.170	5.05	4.69	
10 h	244	56.0	73.3	219	0.00337	1.48	0.173	0.179	5.14	4.79	

*The α_S -plots are available as Supplementary Information (Fig. S4)

a_{BET} = specific area obtained by the BET method

V_m = maximum volume of adsorbed N₂, at standard temperature and pressure, for monolayer formation

C = BET constant (dimensionless)

$a_{ext-mier}$ = remaining area after micropore filling

V_{micro} = volume of micropores

$a_{ext-mes}$ = remaining area after all pores were filled

V_{total} = total volume of pores

n.d. = not determined

tungsten was associated to unreacted ZrW_2O_8 particles. The reacting suspensions remained opaque during the entire synthesis process and, therefore, there was no visual clue that a solubilization-precipitation process was involved in the formation of nanocrystalline hydrous zirconia.

These previous assumptions on the mechanism of formation of hydrous zirconia from zirconium tungstate were now put to the test based on an extensive set of experiments under different synthesis conditions. First of all, it now seems that the presence of residual tungsten in all hydrous zirconia samples (Table 1) may be explained by some tungstate ions bonded to the zirconia nanoparticles. In fact, there is no evidence of ZrW_2O_8 or WO_3 in the XRD pattern of the synthesized samples, except for the sample produced by 5 min, whose XRD pattern exhibited some minor WO_3 Bragg peaks, as previously mentioned (Fig. 2a). Moreover, even after only 5 min of reaction, the product's XRD pattern is already completely different to that of the precursor, thus indicating that the reaction is very fast, contrarily to what was previously thought. Accordingly, one can infer that the residual tungsten may be present in the crystal structure of zirconia or, more likely, on its surface, helping to stabilize the cubic and tetragonal phases. Those particles with little or no tungsten in the composition possibly consist of monoclinic zirconia (Fig. 1d).

Low magnification scanning electron micrographs (Fig. 6) suggest that particle size and morphology remain essentially unaltered with the reaction. Micrographs at higher magnifications, however, show the presence of nearly spherical particles (5 nm) much smaller than the primary particles of ZrW_2O_8 (1.7 μm) (Table 4). Moreover, the analysis of the α_S -plot (Fig. S4) suggests an increase in the external area of the samples (Table 4). One may thus conclude that the synthesis of hydrous zirconia from zirconium tungstate cannot proceed through a topotactic reaction, wherein porosity increases by removing part of the structure while external area and particle size remain unaltered (Alario Franco and Sing 1974).

Based on the experimental evidence gathered in this work, the production of nanocrystalline hydrous zirconia from ZrW_2O_8 in NaOH aqueous solution may be understood as follows. In the first step, OH^- ions react with ZrW_2O_8 giving WO_4^{2-} and highly hydrated/hydroxylated zirconium structures. These hydroxylated species further undergo condensation reactions with the elimination of water molecules,

giving rise to Zr-O-Zr bonding and structuring into small crystallites of zirconia.

Parallel to this two-steps mechanism, it cannot be ruled out a possible contribution from a solubilization/precipitation route. Indeed, some portions of the material reacted in aqueous NaOH solution can be hydroxylated to the point of yield complex zirconium ions of the type $\text{Zr}(\text{OH})_5^-$ and $\text{Zr}(\text{OH})_6^{2-}$, soluble in the alkaline medium and forming colloidal species (Antunes 2016). Indeed, according to the zirconium ion solubility diagram proposed by Mompean et al. (2005), if only 30% of the initial mass of ZrW_2O_8 were solubilized in the reaction with NaOH, the concentration of Zr^{4+} ions (about 10^{-3} mol L^{-1}) would be sufficient for the formation of polynuclear species or colloidal precipitates of zirconia. The formation of colloidal zirconium species was also observed by Cho et al. (2005) and Kobayashi (2010), who determined the solubility of $\text{Zr}(\text{OH})_4$ and ZrO_2 at different pH values. Monoclinic zirconia particles (already present in the precursor - as verified by XRD), which does not solubilize easily, as well as the newly formed nanocrystalline zirconia agglomerates, can act as heterogeneous nucleation sites, facilitating the precipitation of complex zirconium ions. With the progress of polymerization/condensation reactions, these colloidal species may also undergo Zr-O-Zr bonding, thus contributing to the formation of zirconia crystallites.

Increasing reaction time and temperature are factors that facilitate the condensation of hydroxyl groups and formation of Zr-O-Zr bonds, with the release of water molecules (Chuah 1999). Zr-O-Zr bonding can also be promoted by the presence of OH^- ions in the medium, which act deprotonating the surface hydroxyls present in the hydrous oxide. The residual positive charge on the zirconium makes it prone to make a bond to oxygen ions on the surface of adjacent colloids.

The maximum crystallite size for the hydrous zirconia samples obtained in this study was approximately 3 nm (Table 1). The stabilization of zirconia at such a small crystallite size is probably linked to some residual tungsten and sodium ions, as previously suggested, respectively, in studies conducted by Cortés-Jácome et al. (2002) and Lara-García et al. (2014). The presence of such residual chemical species possibly reduces the surface energy of the crystallites, interfering with its growth, and further contributes to the stabilization of tetragonal/cubic phase of zirconia as a nanoscale effect.

Samples produced for 5 min to 1 h and 8 h (with NaOH 1 mol L⁻¹ at 80 °C), and at 60 and 100 °C (with NaOH 2 mol L⁻¹ to 5 h) exhibited an exothermic DSC peak around 450–550 °C (Table 3) accompanied by loss of water and CO₂. According to the literature, this exothermic peak can be assigned to crystallization of an amorphous fraction to the tetragonal phase (Chuah 1999; Nawrocki et al. 1993; Chen et al. 2009). Besides, this exothermic peak may also result from the cubic to tetragonal zirconia phase transition. This phase transition may be triggered by a slight increase in crystallite size with the elimination of surface water/hydroxyl and CO₂, which were stabilizing the cubic phase by reducing the specific surface energy.

The hydrous zirconia surface areas obtained by BET, greater than 30,000 m² mol⁻¹ (assuming a molecular weight of 143 g mol⁻¹), put these samples in the region of the nanocrystalline zirconia phase diagram in which the amorphous phase should be thermodynamically stable Pitcher et al. (2005). However, phase stability may be altered by the presence of tungsten and sodium contaminants, in addition to water and CO₂ adsorbed at the particles surface. The presence of such chemical species affects the zirconia nanoparticles surface energy, to the point that cubic zirconia (identified by Raman spectroscopy in all samples regardless synthesis conditions) may become more stable than the amorphous phase in crystallites less around 3 nm in diameter.

Although the cubic phase is not included in the diagram proposed by Pitcher et al. (2005), Tsunekama et al. (2003) observed the transition from cubic to tetragonal zirconia in 2.05 ± 0.15 nm crystallites having a O:Zr ratio of 1.792. Thus, given the presence of Na and W contaminants, along with the high degree of hydration/hydroxylation and carbon dioxide adsorbed at the surface, as well as the unusually small crystallite size, it is reasonable to suppose that the amorphous, cubic and tetragonal phases of zirconia may be simultaneously present in samples produced from alkaline attack of zirconium tungstate, as demonstrated by the results obtained in this work.

Regarding the true density reported in Table 4, the reduction of the nanocrystalline zirconia density to values close to 5 g cm⁻³ can be understood in terms of the presence of a hydroxide layer on the particles surface, an effect that is more pronounced as the particle size is less than 50 nm (Opalinska et al. 2015). In a

previous study, it was found that samples composed of 11 nm zirconia particles had a true density of 5.22 g cm⁻³ (Opalinska et al. 2015). Accordingly, samples consisting of particles with sizes below 10 nm and specific areas higher than 100 m² g⁻¹ should have a true density of less than 5.20 g cm⁻³, in agreement with the results here reported.

Conclusions

The production of zirconia in the form of a hydroxylated/hydrated material from the ZrW₂O₈ is a rapid and spontaneous process in a highly alkaline environment (pH > 13) even at moderate temperatures (60 °C) and for short periods of time (5 min). The morphology of the particulate materials obtained under different synthesis conditions was not affected by NaOH concentration, temperature and reaction time. In fact, all samples consisted of nanoparticle agglomerates of various sizes and shapes, with irregular surfaces, high specific areas and mesoporosity, with a strong tendency to adsorption of water and carbon dioxide. Also, all samples, regardless synthesis conditions, had Raman spectra similar to that of nanocrystalline cubic zirconia with a small contribution of monoclinic phase (already present as an impurity in the precursor material).

As the NaOH concentrations employed always provided an excess of OH⁻ ions in the medium and pH values higher than 13, this parameter did not significantly affect the resulting products. On the other hand, upon increasing reaction time and temperature, the products tend to exhibit a more ordered and condensed structure. This also impacts on the onset temperature for elimination of water and CO₂ in the evolved gases in thermal analysis. Temperature and reaction time provides a mean to control the amount of residual tungsten and the crystallite size, which afforded materials rich in tetragonal zirconia, with crystallites lower than 15 nm, after treatment at 1000 °C under an inert atmosphere.

The proposed synthesis mechanism of hydrous zirconia from zirconium tungstate involves the replacement of WO₄ by OH groups, accompanied by some degree of solubilization of the zirconia structure due to high hydroxylation of its surface, yielding colloidal species which give rise to crystallites with a structure similar to that of cubic zirconia. Colloidal species of complex zirconium ions polymerize/condense via a mechanism facilitated by heterogeneous nucleation

due to the presence of monoclinic zirconia nuclei and the high saturation of the medium, which promotes nucleation over growth. Thus, the size of the zirconia crystallites remains around 3 nm. The presence of some residual sodium and tungsten, along with water/hydroxyls and carbon dioxide adsorbed on the surface, may also contribute to the stabilization of the cubic phase by reducing the surface energy of such small hydrous zirconia crystallites.

Acknowledgments The authors acknowledge financial support from the Brazilian agencies Fundação de Amparo à Pesquisa do Rio Grande do Sul (FAPERGS), Coordenação de Aperfeiçoamento de Pessoal de Nível Superior (CAPES), Conselho Nacional de Desenvolvimento Científico e Tecnológico (CNPq, research grants #304831/2014-0 (CAP) and #304675/2015-6 (JEZ)), and Secretaria de Desenvolvimento Econômico, Ciência e Tecnologia do Estado do Rio Grande do Sul (SDECT). Thanks are due also to Netzsch Gerätebau GmbH, Fernanda Miotto (Universidade de Caxias do Sul), João Fiori and Rebecca Lewin (Bruker AXS GmbH) for X-ray microfluorescence analysis, and also to the staff of the Laboratório Central de Microscopia Professor Israel Baumvol (LCMic/UCS) and Instituto de Materiais Cerâmicos (IMC/UCS), particularly Robinson C. D. Cruz, Daniel Golle and Márcia Raquel H. Wendler, for technical assistance and helpful discussions.

Compliance with ethical standards

Conflict of interest The authors declare that they have no conflict of interest.

References

- Aguila G, Guerrero S, Gracia F, Araya P (2006) Improvement of the thermal stability of hydrous zirconia by post-synthesis treatment with NaOH and NH₄OH solutions. *Appl Catal A-Gen* 305(2):219–232. <https://doi.org/10.1016/j.apcata.2006.03.025>
- Alario Franco MA, Sing KSW (1974) Propriedades químicas de superficie de los óxidos e hidróxidos de cromo. I. Adsorción de tetracloruro de carbon en el oxí-hidróxido ortorrómbico y sus productos de decomposición. *An Quim* 70:41–48
- Antunes M (2016) Produção, dispersão e consolidação de zircônia obtida a partir do tungstato de zircônio. Doctoral Thesis. Pós-Graduação em Engenharia e Ciência dos Materiais – Universidade de Caxias do Sul, Caxias do Sul, 130 f
- Bachiller-Baeza B, Rodriguez-Ramos I, Guerrero-Ruiz A (1998) Interaction of carbon dioxide with the surface of zirconia polymorphs. *Langmuir* 14(13):3556–3564. <https://doi.org/10.1021/la970856q>
- Balzar D, Popa NC (2002) Improved modeling of residual strain/stress and crystallite-size distribution in Rietveld refinement. *Adv X-ray Anal* 45:152–157
- Barrett EP, Joyner LG, Halenda PP (1951) The determination of pore volume and area distributions in porous substances. I. Computations from nitrogen isotherms. *J Am Chem Soc* 73(1):373–380. <https://doi.org/10.1021/ja01145a126>
- Blesa MA, Maroto AJG, Passaggio SI, Figliolia NE, Rigotti G (1985) Hydrous zirconium dioxide: interfacial properties, the formation of monodisperse spherical particles, and its crystallization at high temperatures. *J Mater Sci* 20(12):4601–4609. <https://doi.org/10.1007/BF00559350>
- Castro RHR, Marcos PJB, Lorriaux A, Steil MC, Gengembre L, Roussel P, Gouvea D (2008) Interface excess and polymorphic stability of nanosized zirconia-magnesia. *Chem Mater* 20(10):3505–3511. <https://doi.org/10.1021/cm703599r>
- Chaplot SL (2005) Negative thermal expansion in ZrW₂O₈—do we give up the concept of normal mode? *Curr Sci India* 88: 347–349
- Chen C-W, Yang X-S, Chiang AST (2009) An aqueous process for the production of fully dispersible t-ZrO₂ nanocrystals. *J Ta Inst Chem Eng* 40:296–301
- Chitrakar R, Tesuka S, Sonoda A, Sakane K, Ooi K, Hirotsu T (2006) Selective adsorption of phosphate from seawater and wastewater by amorphous zirconium hydroxide. *J Colloid Interf Sci* 297(2):426–433. <https://doi.org/10.1016/j.jcis.2005.11.011>
- Cho H-R, Walther C, Rothe J, Neck V, Denecke MA, Dardenne K, Fanghänel T (2005) Combined LIBD and XAFS investigation of the formation and structure of Zr(IV) colloids. *Anal Bioanal Chem* 383(1):28–40. <https://doi.org/10.1007/s00216-005-3354-6>
- Chuah GK (1999) An investigation into the preparation of high surface area zirconia. *Catal Today* 49(1-3):131–139. [https://doi.org/10.1016/S0920-5861\(98\)00417-9](https://doi.org/10.1016/S0920-5861(98)00417-9)
- Chuah GK, Jaenicke S (1997) The preparation of high surface area zirconia—influence of precipitating agent and digestion. *Appl Catal A-Gen* 163(1-2):261–273. [https://doi.org/10.1016/S0926-860X\(97\)00103-8](https://doi.org/10.1016/S0926-860X(97)00103-8)
- Chuah GK, Jaenicke S, Pong BK (1998) The preparation of high-surface-area zirconia. II. Influence of precipitating agent and digestion on the morphology and microstructure of hydrous zirconia. *J Catal* 175(1):80–92. <https://doi.org/10.1006/jcat.1998.1980>
- Clearfield A (1964) Crystalline hydrous zirconia. *Inorg Chem* 3(1):146–148. <https://doi.org/10.1021/ic50011a034>
- Cortés-Jácome MA, Toledo-Antonio JA, Armendáriz H, Hernández I, Bokhimiz X (2002) Solid solutions of WO₃ into zirconia in WO₃-ZrO₂ catalysts. *J Solid State Chem* 164(2):339–344. <https://doi.org/10.1006/jssc.2001.9488>
- Daramola DA, Muthuvel M, Botte GG (2010) Density functional theory analysis of Raman frequency modes of monoclinic zirconium oxide using Gaussian basis sets and isotopic substitution. *J Phys Chem B* 114(29):9323–9329. <https://doi.org/10.1021/jp9077135>
- Delhez R, de Keijser TH, Langford JJ, Louër D, Mittermeijer EJ, Sonneveld EJ (1993) Crystal imperfection broadening and peak shape in Rietveld method. In: Young RA (ed) *The Rietveld method*. Oxford University Press, New York, pp 147–148
- Dell’Agli G, Colantuono A, Mascolo G (1999) The effect of mineralizers on the crystallization of zirconia gel under

- hydrothermal conditions. *Solid State Ionics* 123(1-4):87–94. [https://doi.org/10.1016/S0167-2738\(99\)00109-5](https://doi.org/10.1016/S0167-2738(99)00109-5)
- Dell'Agli G, Mascolo G, Mascolo MC, Pagliuca C (2008) Drying effect on thermal behavior and structural modifications of hydrous zirconia gel. *J Am Ceram Soc* 91(10):3375–3379. <https://doi.org/10.1111/j.1551-2916.2008.02635.x>
- Deshmane VG, Adewuyi YG (2012) Synthesis of thermally stable, high surface area, nanocrystalline mesoporous tetragonal zirconium dioxide (ZrO_2): effects of different process parameters. *Micropor Mesopor Mat* 148(1):88–100. <https://doi.org/10.1016/j.micromeso.2011.07.012>
- Djuraro E, Bouvier P, Lucazeau G (2000) Crystallite size effect on the tetragonal-monoclinic transition of undoped nanocrystalline zirconia studied by XRD and Raman spectrometry. *J Solid State Chem* 149(2):399–407. <https://doi.org/10.1006/jssc.1999.8565>
- Gubanov NN, Baranchikov AY, Kopitsa GP, Almásy L, Angelov B, Yaprıntsev AD, Rosta L, Ivanov VK (2015) Combined SANS and SAXS study of the action of ultrasound on the structure of amorphous zirconia gels. *Ultrason Sonochem* 24: 230–237. <https://doi.org/10.1016/j.ultrasonch.2014.11.012>
- Hannink RHJ, Kelly PM, Muddle BC (2000) Transformation toughening in zirconia-containing ceramics. *J Am Ceram Soc* 83:461–487
- Huang C, Tang Z, Zhang Z (2001) Differences between zirconium hydroxide ($Zr(OH)_4 \cdot nH_2O$) and hydrous zirconia ($ZrO_2 \cdot nH_2O$). *J Am Ceram Soc* 84:1637–1638
- Jaenicke S, Chuah GK, Raju V, Nie YT (2008) Structural and morphological control in the preparation of high surface area zirconia. *Catal Surv Jpn* 12(3):153–169. <https://doi.org/10.1007/s10563-008-9048-2>
- Jiao X, Chen D, Xiao L (2003) Effects of organic additives on hydrothermal zirconia nanocrystallites. *J Cryst Growth* 258(1-2):158–162. [https://doi.org/10.1016/S0022-0248\(03\)01473-8](https://doi.org/10.1016/S0022-0248(03)01473-8)
- Kim B-K, Hamaguchi H-O (1997) Mode assignments of the Raman spectrum of monoclinic zirconia by isotopic exchange technique. *Phys Status Solidi B* 203(2):557–563. [https://doi.org/10.1002/1521-3951\(199710\)203:2<557::AID-PSSB557>3.0.CO;2-C](https://doi.org/10.1002/1521-3951(199710)203:2<557::AID-PSSB557>3.0.CO;2-C)
- Kobayashi T (2010) Solubility of zirconium and thorium in aqueous solutions containing organic acids. Master's thesis. Kyoto University, Kyoto, 121 f
- Köck E-M, Kogler M, Bielz T, Klötzer B, Penner S (2013) In situ FT-IR spectroscopic study of CO_2 and CO adsorption on Y_2O_3 , ZrO_2 , and yttria-stabilized ZrO_2 . *J Phys Chem C* 117(34):17666–17673. <https://doi.org/10.1021/jp405625x>
- Langford JI, Louër D, Scardi P (2000) Effect of a crystallite size distribution on X-ray diffraction line profiles and whole-powder-pattern fitting. *J Appl Crystallogr* 33(3):964–974. <https://doi.org/10.1107/S002188980000460X>
- Lara-García HA, Romero-Ibarra IC, Pfeiffer H (2014) Hierarchical Na-doped cubic ZrO_2 synthesis by a simple hydrothermal route and its application in biodiesel production. *J Solid State Chem* 218:213–220. <https://doi.org/10.1016/j.jssc.2014.06.040>
- Lind C (2012) Two decades of negative thermal expansion research: where do we stand? *Materials* 5(12):1125–1154. <https://doi.org/10.3390/ma5061125>
- Manicone PF, Iommetti PR, Raffaelli L (2007) An overview of zirconia ceramics: basic properties and clinical applications. *J Dent* 35(11):819–826. <https://doi.org/10.1016/j.jdent.2007.07.008>
- Marczewski AW (2002) A practical guide to isotherms of adsorption on heterogeneous surfaces. Available at: <<http://adsorption.org/awm/ads/Ads.htm>>. Access: April 20th, 2016
- Marković JP, Milonjić SK (2006) Synthesis of zirconia colloidal dispersions by forced hydrolysis. *J Serb Chem Soc* 71:613–619
- Matsui K, Ohgai M (2002) Formation mechanism of hydrous zirconia particles produced by hydrolysis of $ZrOCl_2$ solutions. IV-effects of $ZrOCl_2$ concentration and reaction temperature. *J Am Ceram Soc* 85:545–553
- Mompean FJ, Perrone J, Illemassène M (Ed.) (2005) Chemical thermodynamics of zirconium. Elsevier, Amsterdam, volume 8
- Morterra C, Orio L (1990) Surface characterization of zirconium oxide. II. The interaction with carbon dioxide at ambient temperature. *Mater Chem Phys* 24(3):247–268. [https://doi.org/10.1016/0254-0584\(90\)90089-S](https://doi.org/10.1016/0254-0584(90)90089-S)
- Nawrocki J, Rigney MP, McCormick A, Carr PW (1993) Chemistry of zirconia and its use in chromatography. *J Chromatogr A* 657(2):229–282. [https://doi.org/10.1016/0021-9673\(93\)80284-F](https://doi.org/10.1016/0021-9673(93)80284-F)
- Opalinska A, Malka I, Dzwolak W, Chudoba T, Presz A, Lojkowski W (2015) Size-dependent density of zirconia nanoparticles. *Beilstein J Nanotech* 6:27–35. <https://doi.org/10.3762/bjnano.6.4>
- Palmer DA, Eldik RV (1983) The chemistry of metal carbonate and carbon dioxide complexes. *Chem Rev* 83(6):651–731. <https://doi.org/10.1021/cr00058a004>
- Pan B, Xu J, Wu B, Li Z, Liu X (2013) Enhanced removal of fluoride by polystyrene anion exchanger supported hydrous zirconium oxide nanoparticles. *Envir Sci Tech* 47(16):9347–9354. <https://doi.org/10.1021/es401710q>
- Patil KC, Hedge MS, Rattan T, Aruna ST (2008) Chemistry of nanocrystalline oxide materials: combustion synthesis, properties and applications. World Scientific Publishing, Singapura. <https://doi.org/10.1142/6754>
- Perottoni CA (2000) Transições de fase em compostos de estrutura aberta sob altas pressões. Doctoral Thesis. Instituto de Física, Universidade Federal do Rio Grande do Sul, Porto Alegre. 177 f
- Piskorz W, Grybos J, Zasada F, Cristol S, Paul J-F, Adamski A, Sojka Z (2011) Periodic DFT and atomistic thermodynamic modeling of the surface hydration equilibria and morphology of monoclinic ZrO_2 nanocrystals. *J Phys Chem C* 115(49): 24274–24286. <https://doi.org/10.1021/jp2086335>
- Piskorz W, Grybos J, Zasada F, Zapala P, Cristol S, Paul J-F, Sojka Z (2012) Periodic DFT study of the tetragonal ZrO_2 nanocrystals: equilibrium morphology modeling and atomistic surface hydration thermodynamics. *J Phys Chem C* 116(36):19307–19320. <https://doi.org/10.1021/jp3050059>
- Pitcher MW, Ushakov SV, Navrotskyz A, Woodfield BF, Li G, Boerio-Goates J, Tissue BM (2005) Energy crossovers in nanocrystalline zirconia. *J Am Ceram Soc* 88:160–167
- Pokrovski K, Jung KT, Bell AT (2001) Investigation of CO and CO_2 adsorption on tetragonal and monoclinic zirconia. *Langmuir* 17(14):4297–4303. <https://doi.org/10.1021/la001723z>
- Rouquerol F, Rouquerol J, Sing KSW, Llewellyn P, Maurin G (2014) Adsorption by powders and porous solids: principles, methodology and application, 2nd edn. Academic Press, Oxford

- Ross-Medgaarden EI, Wachs IE (2007) Structural determination of bulk and surface tungsten oxides with UV-vis diffuse reflectance spectroscopy and Raman spectroscopy. *J Phys Chem C* 111(41):15089–15099. <https://doi.org/10.1021/jp074219c>
- Shukla S, Seal S (2005) Mechanisms of room temperature metastable tetragonal phase stabilization in zirconia. *Inter Mater Rev* 50(1):45–64. <https://doi.org/10.1179/174328005X14267>
- Silverstein RM, Bassler GC, Morrill TC (1991) Spectrometric identification of organic compounds, 5th edn. John Wiley & Sons, New York, pp 91–164
- Sing KSW, Everett DH, Haul RAW, Moscou L, Pierotti RA, Rouquerol J, Siemieniowska T (1985) Reporting physisorption data for gas/solid systems with special reference to the determination of surface area and porosity. *Pure Appl Chem* 57:603–619
- Sing KSW, Williams RT (2005) Empirical procedures for the analysis of physisorption isotherms. *Adsorpt Sci Technol* 23(10): 839–853. <https://doi.org/10.1260/026361705777641990>
- Somavilla LM, Zorzi JE, Machado G, Ramos GR, de Amorim CLG, Perottoni CA (2011) Nanocrystalline hydrous zirconia from zirconium tungstate. *J Am Ceram Soc* 94(8):2640–2645. <https://doi.org/10.1111/j.1551-2916.2011.04394.x>
- Song Y, Zhang J, Zhang Y, Zhou X, Wang J-A, Xu L (2011) Effect of crystallization mode of hydrous zirconia support on the isomerization activity of Pt/WO₃-ZrO₂. *Catal Today* 166(1): 79–83. <https://doi.org/10.1016/j.cattod.2010.06.002>
- Srinivasan R, Davis BH (1992) Influence of zirconium salt precursors on the crystal structures of zirconia. *Catal Lett* 14(2): 165–170. <https://doi.org/10.1007/BF00765230>
- Srinivasan R, Hubbard CR, Cavin B, Davis BH (1993) Factors determining the crystal phases of zirconia powders: a new outlook. *Chem Mater* 5(1):27–31. <https://doi.org/10.1021/cm00025a009>
- Štefanić G, Štefanić II, Musić S (2000) Influence of the synthesis conditions on the properties of hydrous zirconia and the stability of low-temperature *t*-ZrO₂. *Mater Chem Phys* 65(2): 197–207. [https://doi.org/10.1016/S0254-0584\(00\)00247-9](https://doi.org/10.1016/S0254-0584(00)00247-9)
- Stenina IA, Voropaeva EY, Veresov AG, Kapustin GI, Yaroslavtsev AB (2008) Effect of precipitation pH and heat treatment on the properties of hydrous zirconium dioxide. *Russ J Inorg Chem* 53(3):350–356. <https://doi.org/10.1134/S0036023608030029>
- Stevens R (1986) Zirconia and zirconia ceramics, 2nd edn. Magnesium Elektron, Twickenham
- Tahir MN, Gorgishvili L, Li J, Gorelik T, Kolb U, Nasdala L, Tremel W (2007) Facile synthesis and characterization of monocrySTALLINE cubic ZrO₂ nanoparticles. *Solid State Sci* 9(12):1105–1109. <https://doi.org/10.1016/j.solidstatesciences.2007.07.033>
- Tai CY, Hsiao B-Y, Chiu H-Y (2004) Preparation of spherical hydrous-zirconia nanoparticles by low temperature hydrolysis in a reverse microemulsion. *Colloids Surfaces A* 237(1-3): 105–111. <https://doi.org/10.1016/j.colsurfa.2004.02.014>
- Tang X, Zheng X (2004) Raman scattering and *t*-phase lattice vibration of 3% (mole fraction) Y₂O₃-ZrO₂. *J Mater Sci Technol* 20:485–489
- Tsunekama S, Ito S, Kawazoe Y, Wang J-T (2003) Critical size of the phase transition from cubic to tetragonal in pure zirconia nanoparticles. *Nano Lett* 3(7):871–875. <https://doi.org/10.1021/nl034129t>
- Vural İ (2011) Synthesis of zirconium tungstate and its use in composites with tunable thermal expansion coefficient. Master's thesis. School of Natural and Applied Sciences, Middle East Technical University, Ankara, 149 f
- Wang H, Li G, Xue Y, Li L (2007) Hydrated surface structure and its impacts on the stabilization of *t*-ZrO₂. *J Solid State Chem* 180(10):2790–2797. <https://doi.org/10.1016/j.jssc.2007.08.015>